Electrical impulse characterization along actin filaments in pathological conditions

Christian Hunley, Md Mohsin, Marcelo Marucho

Department of Physics and Astronomy, The University of Texas at San Antonio, San Antonio, TX 78249-5003, USA

Abstract

We present an interactive Mathematica notebook that characterizes the electrical impulses along actin filaments in both muscle and non-muscle cells for a wide range of physiological and pathological conditions. The program is based on a multi-scale (atomic $\rightarrow$ monomer $\rightarrow$ filament) approach capable of accounting for the atomistic details of a protein molecular structure, its biological environment, and their impact on the travel distance, velocity, and attenuation of monovalent ionic wave packets propagating along microfilaments. The interactive component allows investigators to conduct original research by choosing the experimental conditions (intracellular Vs in vitro), nucleotide state (ATP Vs ADP), actin isoform (alpha, gamma, beta, and muscle or non-muscle cell), as well as, a conformation model that covers a variety of mutants and wild-type (the control) actin filament. The simplicity of the theoretical formulation and the high performance of the Mathematica software enable the analysis of multiple conditions without computational restrictions. These studies may provide an unprecedented molecular understanding of why and how age, inheritance, and disease conditions induce dysfunctions in the biophysical mechanisms underlying the propagation of electrical signals along actin filaments.

Keywords: actin filament; electrical signal propagation, soliton; scientific software; pathological conditions; electrical neuron activities.

1. Introduction

Actin filaments are a major component of the cytoskeleton, and essential for various biological activities in eukaryotic cellular processes such as directional growth, shape, division, plasticity, and migration [1, 2, 3, 4, 5]. Recent research on the electrical properties of actin under in vitro conditions revealed an unprecedented role for the microfilaments as bionanowires capable of propagating ionic information [6]. This finding may provide new insights on many electrical processes taking place within smooth muscle, skeletal, and cardiac cells near the membrane or in the nucleus. Furthermore, an additional information delivery system in neuronal cells might be beneficial for intracellular communication in dendrites, the soma, axon, and axon terminal [7]. Indeed, further clarification on the electrical conductivity and ionic transmission properties of actin filaments is vital for a complete understanding of their contributions to cellular functions and information transfer inside cells.

The use of conventional computational tools and approaches to study the interplay between the polyelectrolyte properties of polymer chains and their biological environment break down for cytoskeleton filaments, because they are limited by their approximations and computational cost

Email address: marcelo.marucho@utsa.edu (Marcelo Marucho)

[8]. We recently introduced an accurate and efficient multi-scale theory (atomic $\rightarrow$ monomer $\rightarrow$ filament) that overcomes some of these limitations when investigating electrical signal propagation along single wild-type actin filaments in physiological conditions [9]. The electrical signal that characterizes ion wave packets was shown to propagate as a monotonically decreasing soliton [10]. For the range of voltage stimuli and electrolyte solutions typically present in intracellular and in vitro conditions, the approach was able to predict a lower electrical conductivity with higher linear capacitance and non-linear accumulation of charge under the intracellular conditions. Additionally, the results showed a significant influence of the voltage input on the electrical impulse shape, attenuation, and packet propagation velocity. The filament sustained the soliton propagation at almost constant velocity for in vitro conditions, whereas intracellular conditions displayed a remarkable deceleration. Furthermore, the solitons were narrower and traveled faster at higher voltage input. As a unique feature, the multi-scale theory is able to account for the molecular structure conformation and biological environment changes often present in pathological conditions.

In this work, we present a Mathematica notebook, [11] which utilizes an extension of the multi-scale approach, for an in depth study of monovalent ion wave packets traveling along single actin filaments in a variety molecular conformations and biological environments (https://github.com/MarceloMarucho/SignalPropagationPathologicalCondition). The program performs on single computers at very low computational cost, and does not require specialized training in computational methods, which can often be an obstacle for many students, researchers, and even experts in the field. Specific analyses can be achieved by making changes to the physiological and pathological conditions when selecting the desired nucleotide state (ATP or ADP), isoform (alpha-smooth, alpha-skeletal, alpha-cardiac, gamma-smooth, gamma-cytoplasmic, beta-cytoplasmic), and conformation model (wild-type or mutant) of the actin monomer. As a distinctive characteristic, a series of interactive plots are generated to elucidate the impact of pH, voltage input, and temperature on the filament conductivity, electric potential, velocity, peak attenuation and ionic wave packet profile. Overall, the program is fully editable. This feature allows users to change the default electrolyte aqueous solution and filament model parameters provided in the notebook.

In the following section, we describe the changes introduced on the multi-scale approach to study pathological conditions. In section 3, we describe the electric charge model of an actin monomer for different molecular conformations. Section 4 includes the organization, design and implementation of the interactive program. In section 5, we present an illustrative example, while section 6 includes the summary. A general overview of the multi-scale approach applied to a single (alpha-smooth muscle) wild-type actin filament is presented in the appendix. The explicit details of the theory can be found in a preceding article [9].

2. A multi-scale model for pathological conditions and the interactive program

The formulation of the multi-scale approach includes: (1) the atomistic scale; accounts for the pH of the aqueous solution, deprotonation of active residues on the protein, and the ionic composition of the biological environment, (2) the monomeric scale; models the ionic layering next to the charged protein, as well as, resistance to flow of ions in both the radial direction and along the filament, and (3) the filament scale; determines the velocity, acceleration, and soliton profile, along with the maximum travel time and distance of an ionic wave using a transmission line prototype model.

ion species	valence	mobility (u)	bulk conc.	
			intracellular	in vitro
K^+	1	$5.0148 \times 10^{-10} \exp\left[-2.65449\times10^{-20}/K_bT\right]$	140	100
Na^+	1	$3.25164 \times 10^{-10} \exp\left[-2.64948\times10^{-20}/K_bT\right]$	12	-
Cl^-	-1	$3.57995 \times 10^{-10} \exp\left[-2.51681\times10^{-20}/K_bT\right]$	4	100
HPO_4^{2-}	-2	$1.83587 \times 10^{-10} \exp\left[-2.64948\times10^{-20}/K_bT\right]$	74	-

Table 1: Ionic species used in both the intracellular and in vitro conditions. The last two columns represent the default concentrations used in the multi-scale approach for intracellular and in vitro conditions. The mobility is in units of $mol.m^2/J.s$, and K_b and T represent the Boltzmann constant and temperature in Kelvin. The unit for the bulk concentration is mol/m^3.

2.1. Biological solution model

2.1.1. Aqueous solution

The pathological and physiological intracellular temperature gradient has been shown to range from $308K$ to $315K$ in the cytoplasm [12], around 1^oC higher in the nucleus (when compared to the cytoplasm) [13], and around $321K$ at the mitochondria [14]. The interactive notebook allows users to choose a temperature between $298K$ and $320K$. In this work, we account for the temperature dependence of the viscosity μ by using the temperature dependent equation $\log(\mu) = -4.5318 - 247/(140 - T)$, where T represents the temperature in Kelvin and μ the viscosity in $Kg/m.s$ [15].

The relative permittivities for the intracellular and in vitro conditions are set to $80\epsilon_0$ and $78.358\epsilon_0$, respectively, were ϵ_0 is the permittivity of free space.

2.1.2. Electrolyte

In this work, the dynamic mobility u for each ion species is estimated using the temperature dependent function $u(T) = u_0 \exp\left[-U_o/K_bT\right]$ [16, 17]. We obtained the parameters u_0 and U_o using the $FindFit$ Mathematica function [18] and the experimental mobility values for several temperatures [19, 20]. This and other ionic species properties are shown in table 1. For instance, in figure 1a we show the fitting function for the sodium mobility for intermediate temperatures values between $275K$ and $320K$ (solid blue curve) and the corresponding experimental values (red dots).

2.2. Filament model

In table 2 (details are provided in the appendix) we tabulated the electric charge and surface charge density of the Cong molecular structure model [21] for the alpha wild type actin filament using the ATP state in physiological conditions. The intracellular pH for healthy cells lies between 6.8 and 7.3. On the other hand unhealthy cells, such as those infected with cancer, have been seen with a pH value between 7.2 and 7.8. Additionally, Alzheimer's disease (AD) cells have shown a decrease in pH value when compared to healthy cells [22], being 6.5 the lowest pH found in brain ischemia [23]. As a unique feature, the surface charge density for intermediate pH values in the range between 6.0 and 8.0 were accurately estimated using the Mathematica Interpolation function [18], which uses third order fitting polynomial curves between successive data points. For illustration purposes, we display the discrete surface charge density values coming from the molecular structure and those coming from the interpolating function in figure 1b.

2.3. Monomer model

The actin monomer length (l) is set to $5.4nm$. The Mathematica interpolation function was used with surface charge density values to account for the pH dependence of the electric potential, electrical conductivity, resistances and impedance.

pH	14 monomers filament charge [e]	surface charge density σ [C/m^2]
5	23	0.006
6	-82	-0.021
7	-154	-0.039
8	-184	-0.047
9	-222	-0.056

Table 2: The filament surface charge density (SCD) and electric charge obtained from the Cong (https://www.rcsb.org/structure/3B5U) molecular structure model for pH values 5-9, using the ATP state for a single (alpha-smooth muscle) wild-type actin filament. The electric charge was calculated using pdb2pqr webserver with an Amber force field (https://server.poissonboltzmann.org/pdb2pqr).

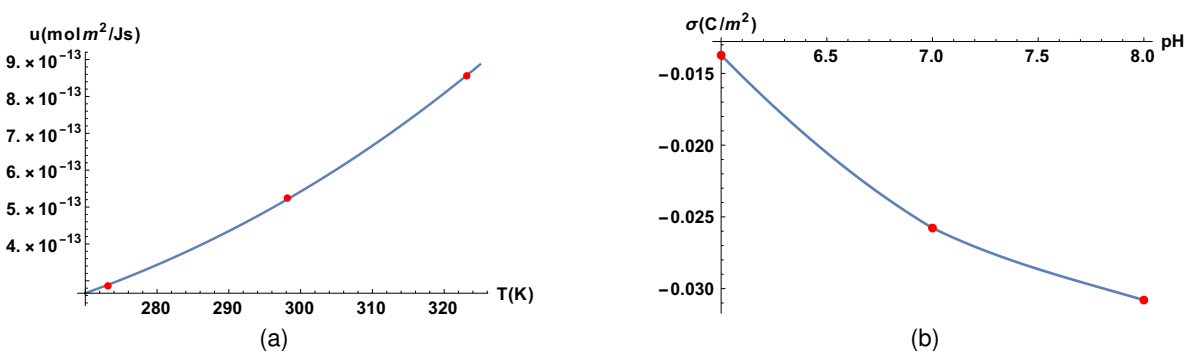

Figure 1: Validation on the Mathematica Interpolation functions. (a) The solid line represents sodium mobility for intermediate temperatures values between $275K$ and $320K$. While, the red dots stand for the corresponding values obtained from experiments. (b) The solid line represents the surface charge density interpolating function for intermediate pH values between pH 6.0 and pH 8.0, whereas, the red dots are the values tabulated in table 1.

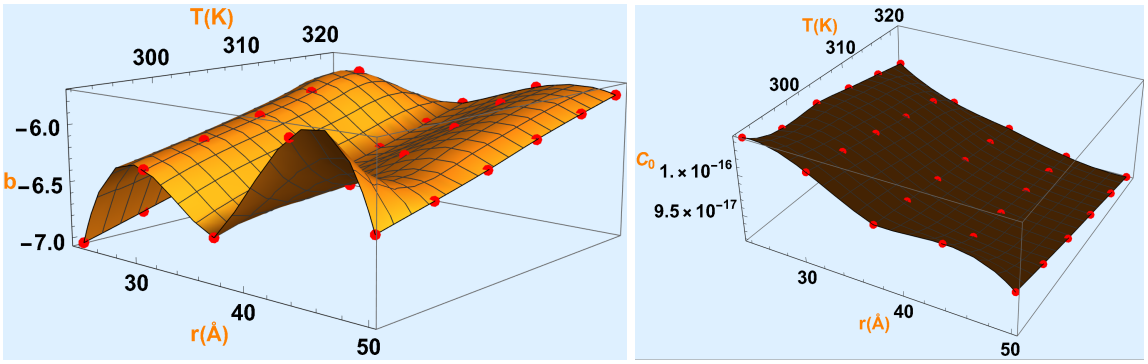

(a) Parameter b (b) Parameter C_o

Figure 2: Capacitance interpolating surface functions for intracellular condition.

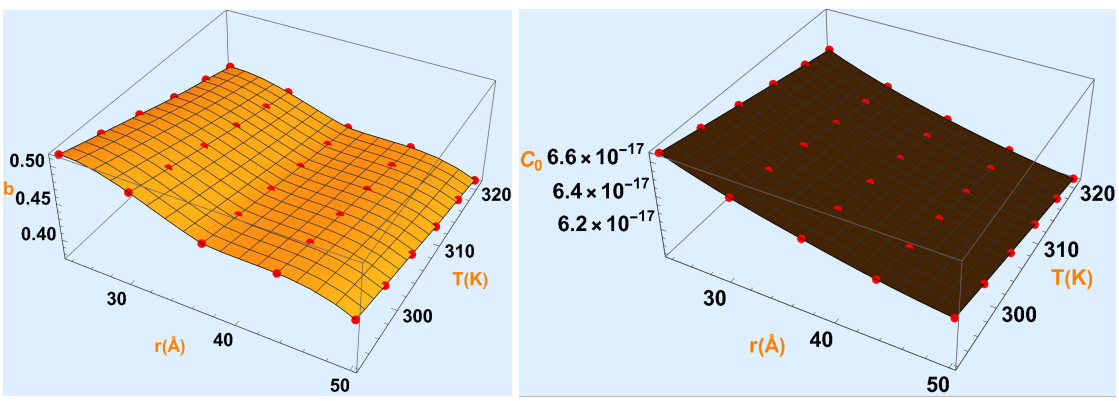

(a) Parameter b (b) Parameter C_o

Figure 3: Capacitance interpolating surface functions for in-vitro condition.

A Java Application for Cytoskeleton Filament Characterization (JACFC) web application [24, 25, 26] was used to obtain the capacitance parameters for different temperatures and filament radii.

A Mathematica interpolation was used to generate interpolating functions for the nonlinear parameter b and capacitance C_0 for temperatures ranging from 292.15K to 321.15K, and filament radii ranging from 23.83Å to 50Å. Surface interpolating functions with JACFC data points are displayed in the plots 2 and 3 for intracellular and in vitro conditions, respectively.

3. Electric charge models for the nucleotide states, isoforms, and missense mutations

In the following subsections, we outline the method for determining the electric charge model for the nucleotide states, isoforms, and missense mutations. We also state the options available in the interactive program when choosing a mutation. A summary of the models is provided in table 3. More information on disease associated with actin, as well as a large list of phenotypes, genes and amino acid mutations can be found in the article by Parker et al. [27].

3.1. Nucleotide states and isoforms

Based on previous studies, we assume that the surface charge density of the alpha wild type filament falls approximately 9% (1/11) when a P_i (phosphorus ion) is released from the wild type

		Muscle		Non-Muscle	
Isoforms	Number of electron charge	**ACTA1**	Number of electron charge	**ACTG1**	Number of electron charge
alpha-smooth	-11	core myopathy	-10	Baraitser-Winter syndrome	-11
alpha-skeletal	-11	nemaline myopathy	-9	Deafness	-8
alapha-cardiac	-11	actin myopathy	-10	**ACTB1**	
gamma-smooth	-10	fetal akinesia	-12	Developmental disability	-9
gamma-cytoskeleton	-10	**ACTA2**		Neutrophil dysfunction	-8
beta-cytoskeleton	-10	falilial thoracic aortic aneurysm	-12		
		dissection syndrome	-10		
		ACTG2			
		MMIHS	-11		
		ACTC1			
		DCM / HCM	-10		

Table 3: Electric charge models for actin protein isoforms and mutations with some associated diseases.

actin filament following hydrolysis of the actin-bound ATP to ADP-P_i. This results in a minus one charge difference between the ATP and ADP actin monomers. An in depth understanding of ATP and ADP actin states can be found in the work by Kudryashov et al. [28]. Similarly, we model gamma-smooth muscle, as well as gamma (γ) and beta (β) non-muscle (cytoplasmic) actin isoforms to have one less net negative charge than alpha (α) actin isoforms according to their amino acid sequence [29].

3.2. Missense mutations

The most common mutation in G-actin comes from missense mutations, which result in a substitution of a single amino acid on the wild-type actin monomer. The substitution on the mutated monomer may come in one of the following amino acid exchanges: (1) amino acid residue $\rightarrow$ different amino acid residue, (2) amino acid residue $\rightarrow$ amino acid, (3) amino acid $\rightarrow$ amino acid residue, or (4) amino acid $\rightarrow$ different amino acid. Here the word "residue" represents an amino acid that is affected by the pH of the solution, and may loose (gain) a hydrogen atom with an increase (decrease) in the pH level. In cases $(1)-(3)$, the type of residue removed and/or added, along with its charge at that pH value, are considered in the calculations of the new monomer surface charge density. On the other hand, in the case (4) there is no change to the electric charge, because the amino acid side chain doesn't respond to the hydrogen concentration of the aqueous solution (i.e. pH of solution). These substitutions are represented using the three letter abbreviation of the amino acid being removed, the residue number, and the abbreviated name for the replacement amino acid (i.e. Abc#Def).

3.2.1. alpha-skeletal

The ACTA1 mutations are recognized in diseases related to skeletal muscle, and have been estimated as 92% missense mutations [30]. Some consequences of these mutations were detected in hypertrophic cardiomyopathy (HCM), congenital myothopy, and muscular dystrophy. Here we consider the ACTA1 mutations representing the core myopathy, nemaline myopathy, actin myopathy, and fetal akinesia. These mutations are the result of the substitutions Asp1Tyr, Glu4Lys, Gly15Arg, and Cys17Arg, respectively.

3.2.2. alpha-smooth muscle

The ACTA2 mutations are known to occur in smooth muscle cells. In this work, the available phenotype options for these mutations are falilial thoracic aortic aneurysm and dissection syndrome (Familial TAAD), which are associated with the amino acid substitutions Gly36Arg and Cys17Arg, respectively.

3.2.3. gamma-smooth muscle

In this interactive notebook we account for ACTG2 mutations by the substitution Arg255Cys, which have demonstrated to have a connection to megacystis microcolon-intestinal hypoperistalsis syndrome(MMIHS).

3.2.4. alpha-cardiac

Cardiac muscle mutations (ACTC1) caused by actin often (not always) result in loosing a positively charged residue and replacing it with a neutral Cys or His residue at the physiological pH values $(6-8)$. Here, we use the substitution Arg210His, which has been know to cause dilated cardiomyopathy (DCM) and hypertrophic cardiomyopathy (HCM).

3.2.5. non-muscle (cytoplasmic)

Finally, we represent two mutations each for the non-muscle (cytoplasmic) missense mutations ACTG1 and ACTB1. The former is recognized in the phenotypes Baraitser-Winter syndrome (Asn10Asp) and deafness (Glu239Lys), whereas the latter is associated with a developmental disability (Met311Arg) and Neutrophil dysfunction (Glu362Lys).

4. Design and implementation

The organization of the Mathematica notebook is presented in Figure 4. In section 1 on the notebook, we defined the electrolyte aqueous solution and filament model parameters described in sections 2 and 3 on this article. While section 2 of the program contains the soliton equations corresponding to the transmission line theory for actin filaments outlined in the appendix. Finally, the interactive plots are provided in section 3 on the notebook.

The initiation of the program is started by clicking the "run notebook" box located at the top of the interactive Mathematica notebook (Figure 5). The program allows for simple to use input parameters (radius and surrounding temperature), along with the choice of actin ATP or ADP assembled monomers, six choices of actin isoforms, and either a wild-type or mutated actin conformation (see Figure 6). If the mutant option is selected, a second screen will open to choose a phenotype (see Figure 7). After the program has completed all computations and rendering of all plots, the last screen will open to notify the user that the calculations are finished (see Figure 8).

4.1. Interactive options

There are three important parameters that can be manipulated in the interactive plots to obtain a more detailed analysis. These are the following: (1) the condition of the biological environment (in vitro or intracellular), (2) the input voltage, and (3) the pH of the electrolyte solution. A brief explanation for each of the three options is given below.

4.1.1. In vitro and Intracellular conditions

All the results can be analyzed at both in vitro and intracellular conditions. In this program, the in vitro environment represents a surrounding aqueous electrolyte solution containing potassium chloride KCl as the electrolyte, and the intracellular model includes potassium chloride KCl, sodium (Na), as well as hydrogenphosephate (HPO_4^{-2}) to represent larger charged anions in the biological environment (see table 1). For the velocity and amplitude attenuation plots, the in vitro and intracellular conditions can be selected independently, or chosen simultaneously. However, there are two sections for the soliton results that represent the in-vitro and intracellular conditions separately.

4.1.2. Voltage input

In some plots, the input voltage is being used to compare in vitro and intracellular conditions, while a pre-defined domain or range is used in others. In the first situation the input voltage cannot be adjusted by the user (see figures 12a and 15). Otherwise, the input voltage can be chosen using the slider for values between $0.05V - 0.4V$ volts. This voltage input range includes the values used in invitro experiments [31, 6]. For the soliton profiles, both in vitro and intracellular sections have an animation that compares two voltage inputs of $0.05V$ and $0.15V$ while the slider represents the change in time.

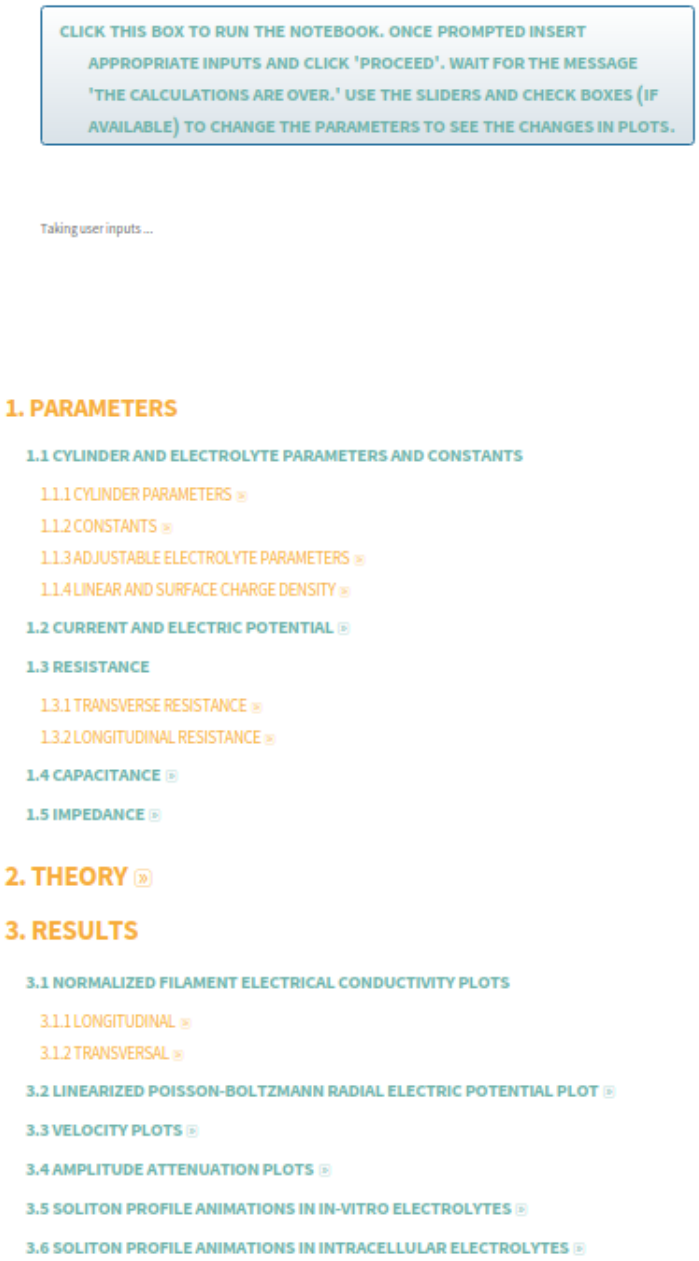

Figure 4: Mathematica notebook content organization

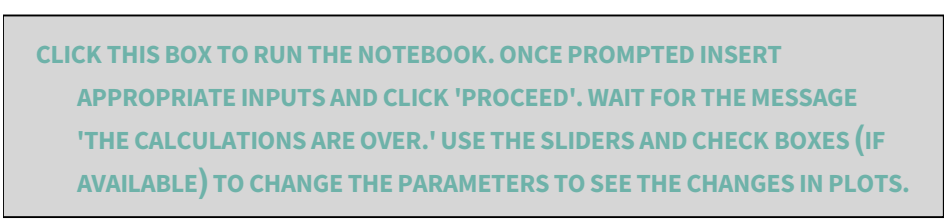

Figure 5: Starting the program: Upon opening the Mathematica notebook the user has to click in the box where it states “Click this box to run the notebook... .”

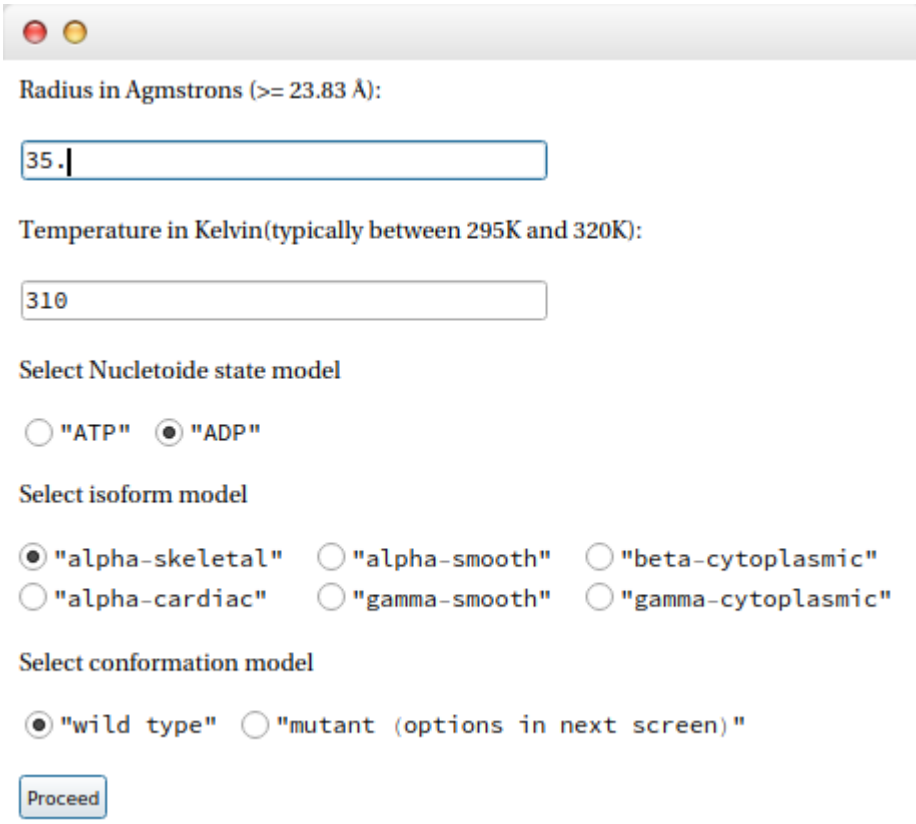

Figure 6: After clicking the “run notebook” box, a dialog box will open and ask the user to set the input parameters (Radius in Angstroms, Temperature in Kelvin, Nucleoide state model, isoform model, and conformation model)

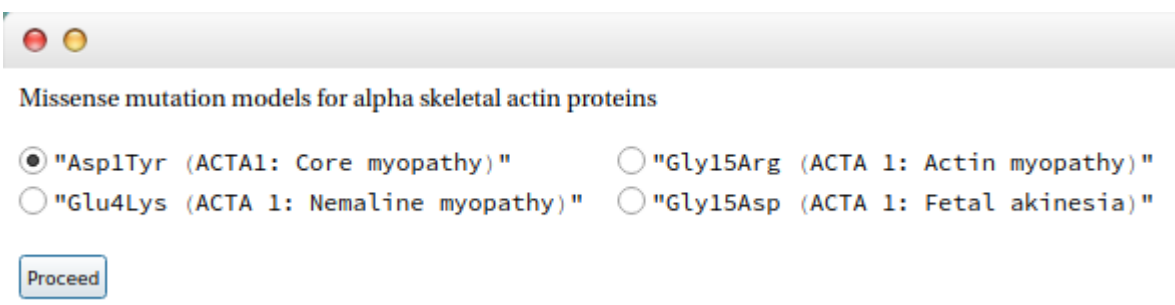

(a)

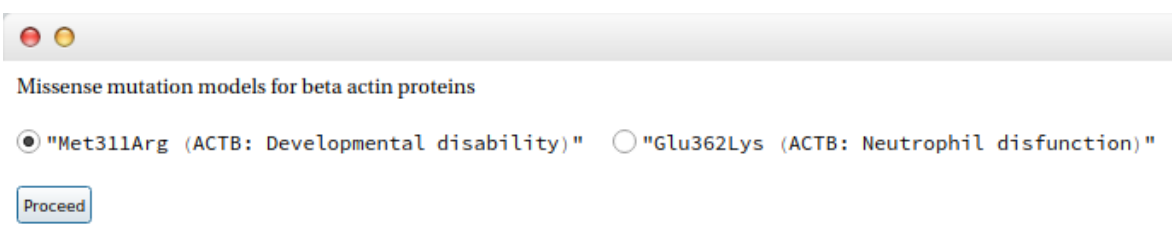

(b)

Figure 7: If the user selects the “mutant” option, a following dialog box will open and ask the user to select the missense mutation (phenotype). According to section 3 on this article, there is different dialog box per each actin isoform. Here we show the missense mutation options after selecting the alpha skeletal isoform (a) or the beta actin isoform (b) in the previous dialog box.

Figure 8: After the program completes all calculations and rendering all plots, a pop-up message will inform the user that “The calculation is over.”

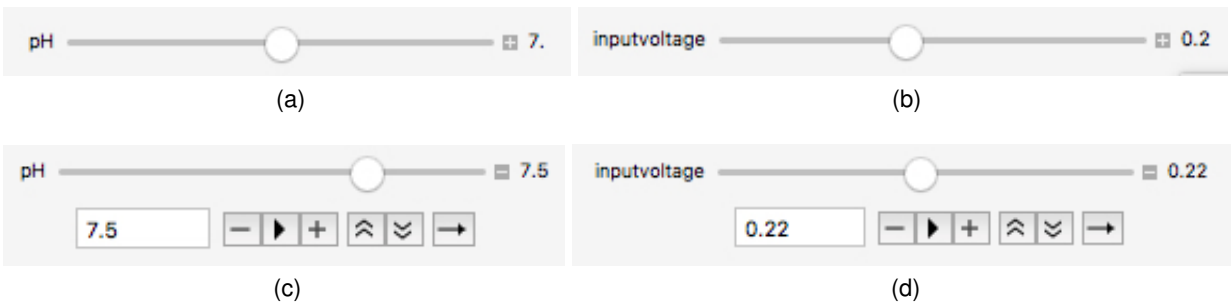

Figure 9: The slider for the respective plots can be changed to fine tune results for a specific analysis. In the sub plots, the slider has been adjusted between the discrete values of $7.0, 7.1, 7.2, 7.3, 7.4$, and 7.5. for pH in plots (a) and (c), and 2.0 and 2.2 for in put voltage in plots (b) and (d).

4.1.3. pH

The interactive notebook allows users to analyze pH solutions in the range between 6.0 and 8.0. A lower pH value comes from a greater number of hydroxide ions in the solution. This means more positively charged hydrogen ions protonate the residues on the actin monomer and decrease the charge of the filament when the G-actin is negative (see table 2). Otherwise, a higher pH decreases the number of hydroxide ions in solution due to deprotonating the active residues on the monomer, which results in an increase in the negative charge of actin. Thereby, pH solution affects the formation of the EDL due to fewer counterions accumulating at the filament surface.

4.1.4. Using the slider

The results in the Radial Electric Potential, Velocity, and Amplitude Attenuation sections include interactive plots with an adjustable slider that allows extensive analyses of the pH and input voltage. The sliders can be adjusted manually by sliding left or right, and also by clicking the “plus” sign at the end of the bar for finer adjustments (Figure 9). Additionally, a pH value can be fine tuned to a tenth of the value desired (Figure 9a, 9c), where as the voltage can be adjusted to two hundredths of the nearest whole number (Figure 9b, 9d).

Illustrative example

For physiological conditions, the Mathematica program reproduces the results and plots provided in reference [9]. Below, we provide the results and a brief analysis for an actin filament of radius equal to 35Å in the ADP nucleotide state and immersed in a electrolyte solution at 310K.

4.2. Relative filament conductivity (to bulk conductivity)

Figure 10 shows the relative filament conductivity results as a function of the pH in both the longitudinal (axial) and transversal (radial) directions. It can be seen that the relative filament con-

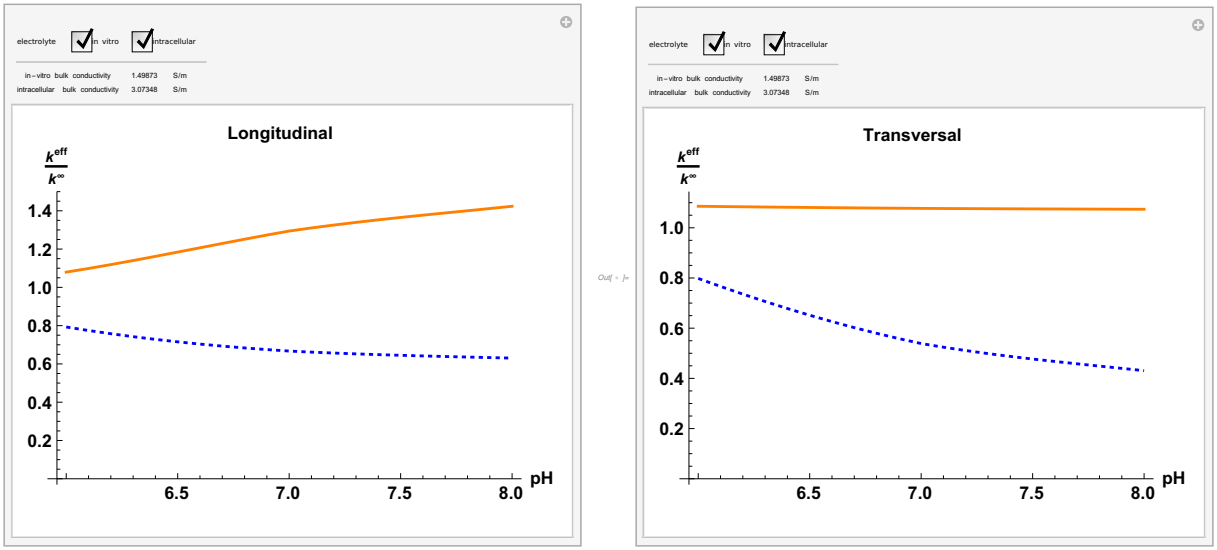

(a) (b)

Figure 10: Relative filament conductivities for both the longitudinal (a) and transversal (b) directions. The orange solid and blue dashed lines correspond to the intracellular and in-vitro conditions, respectively.

ductivity in a in vitro electrolyte aqueous solution (dashed blue curves) is lower than in the intracellular condition (solid orange curves) and decreases with pH for both longitudinal and transversal directions. Whereas, those in intracellular conditions (solid orange) are higher and increases with pH for the longitudinal direction, but remains nearly constant in the radial direction. This behavior was observed in invitro experiments with actin filaments [31].

4.3. Radial electric potential

The absolute value of the linearized Poisson-Boltzmann radial electric potential as a function of the distance is displayed in figure11 for both electrolyte conditions. The subfigure 11a reveals a higher electric potential magnitude in the intracellular condition (orange solid curve) when compared to in vitro condition (blue dashed curve). The slider was used to increase the pH value showing an increasing relationship with the magnitude of the electric potential (subfigure 11b). This is an expected result, because the increase of the pH removes hydrogen ions from amino acid residues and exposes more negative charges on the protein.

4.4. Velocity profiles

The time average velocities are shown as a functions of the voltage input and pH for both electrolyte conditions in subfigures 12a and 12b, respectively. With increasing input voltage, the average velocity remains almost constant for the in vitro condition. Whereas, the average velocity is enhanced with increasing input voltage for the intracellular condition. Additionally, the average velocity increases with pH for the in vitro condition, however, it decreases for the intracellular condition. A decay in the velocity over time is demonstrated in figure 13, and concludes that solitons travel faster under in vitro conditions when compared to intracellular conditions.

4.5. Amplitude attenuation profiles

The first amplitude plot (Figure 14) demonstrates the soliton attenuation while allowing for the input voltage and pH to be adjusted using the slider. The peak of a decreasing soliton profile over

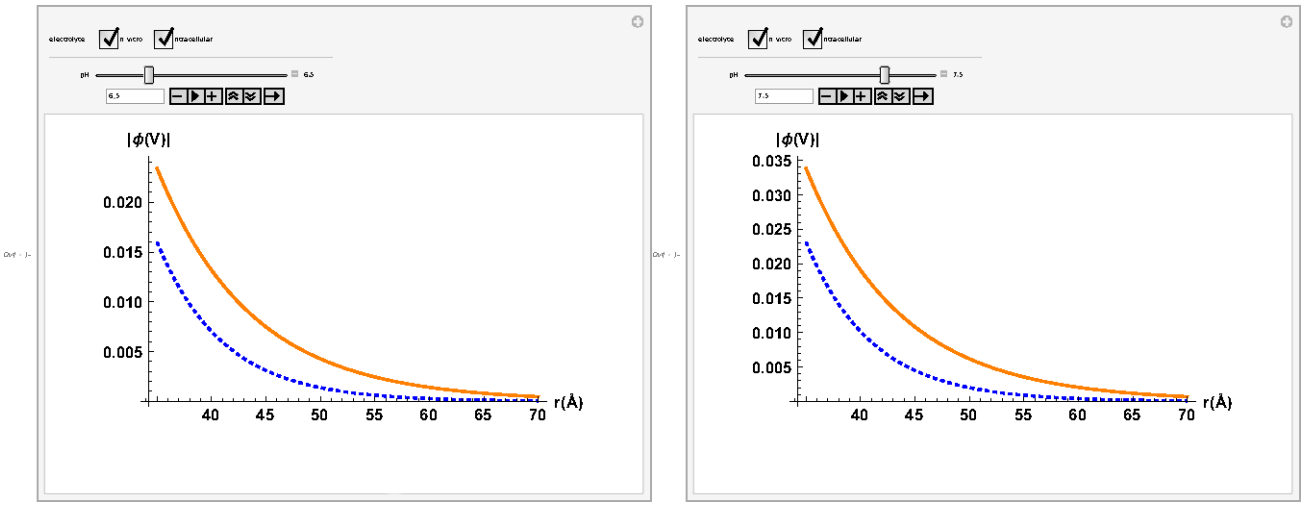

(a) (b)

Figure 11: Absolute value of electrical potential as function of distance from the filament axes. Here plots for pH 6.5 (a) and pH 7.5 (b) are shown by using the slider. The orange solid and blue dashed lines correspond to the intracellular and in vitro conditions, respectively.

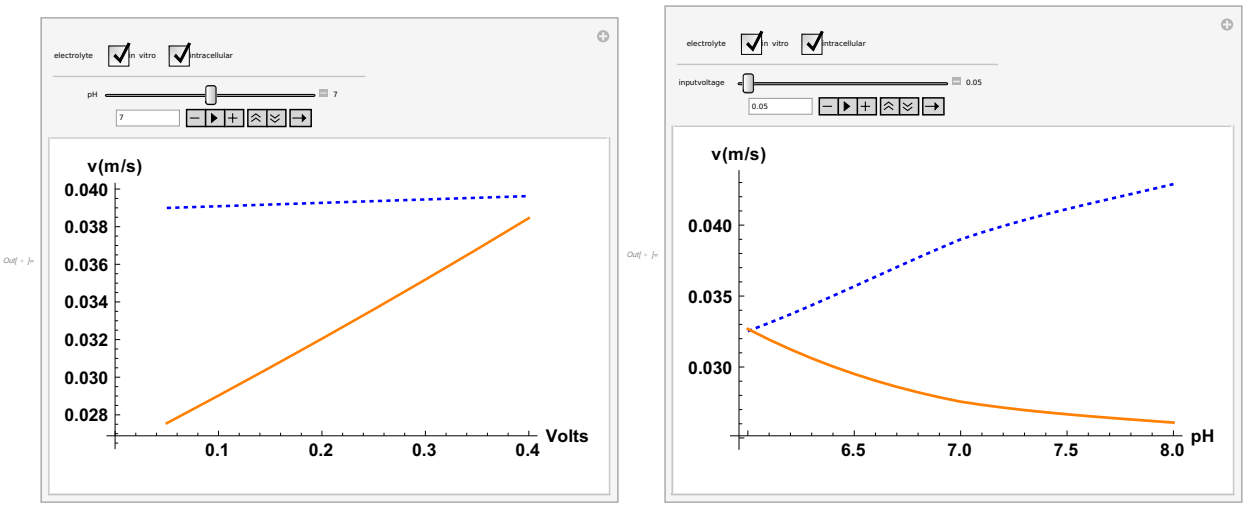

(a) (b)

Figure 12: Average velocities as functions of input voltage for pH 7 (a) and as function of pH for input voltage 0.05V (b). The orange solid and blue dashed lines correspond to the intracellular and in-vitro conditions, respectively.

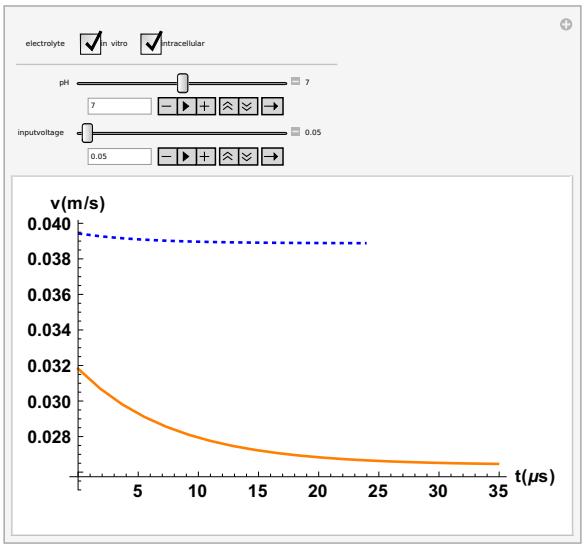

Figure 13: Velocity as a function of time. The orange solid and blue dashed lines correspond to the intracellular and in-vitro conditions, respectively.

time can be analyzed in figure 14. Here the pH of the solution has been adjusted between 6 and 8. For intracellular conditions, a lower pH value results in a faster decay of the soliton due to a weaker electrostatic screening of the EDL (Figure 14a). The result of an increased pH is shown in subfigure 14b, where a soliton peak travels further for intracellular conditions.

The second amplitude attenuation plot (Figure 15) shows the decay of two different soliton peaks with voltage inputs $V_0 = 0.05V$ (dashed curves) and $V_0 = 0.15V$ (solid curves) for in-vitro (blue color) and intracellular (orange color) conditions and pH 7. It can be seen that larger input voltages generate faster amplitude decay rates.

4.6. Soliton animation profiles

By clicking the button(▶), the animations in figures 16, 17, and 18 show how a soliton propagates down the filament length. Figure 16 includes two snapshots of in vitro soliton animations at pH 7. On the other hand, figure 17 includes snapshots of the soliton propagation in intracellular conditions which show a faster soliton at higher voltage input. In figure 18, we show the impact of pH on the soliton profiles in in vitro (a) and intracellular (b) conditions. We noticed that pH does not affect the soliton propagation in in vitro conditions. Whereas, a slightly faster soliton is produced at low pH in intracellular conditions. It can be seen that larger voltage inputs generate higher amplitudes, which is in agreement with experimental studies in invitro conditions [6].

5. Summary

Due to their conducting bionanowire properties, actin filaments have been experimentally demonstrated and theoretically modeled to be capable of transmitting ions across their filament length when a Gaussian input voltage is applied to the filament. The solitons produced by the transmission line model represent ionic waves, which travel distances in the neighborhood of a micron, and could be a biological consequence in the local vicinity of cells [32].

In this work, we introduced an interactive Mathematica notebook that allows for the characterization of the soliton propagation along actin filaments for a wide range of physiological and

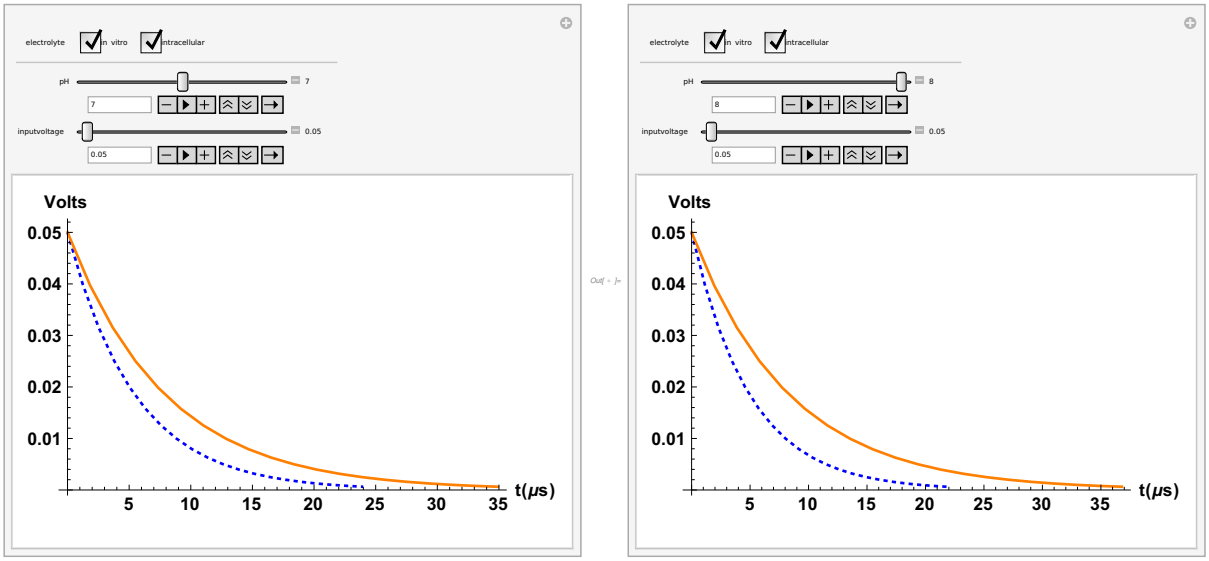

(a) (b)

Figure 14: Soliton peak attenuation as a function of time at a voltage input of $0.05V$ and for pH 7 (a) and pH 8 (b).

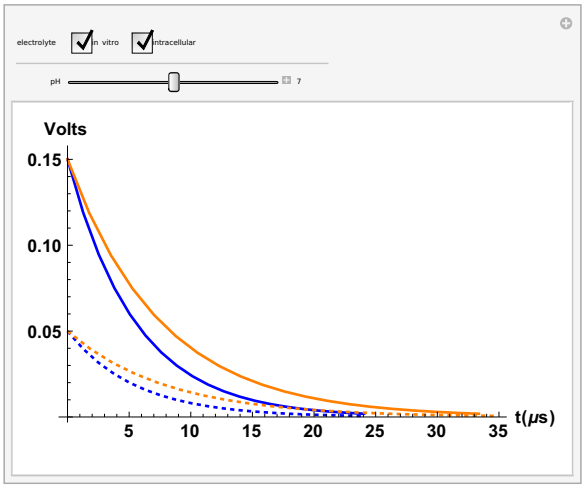

Figure 15: Attenuation of input voltages 0.15 V (solid line) and 0.05 V (dashed line) for in-vitro (blue color) and intracellular (orange color) conditions and pH 7.

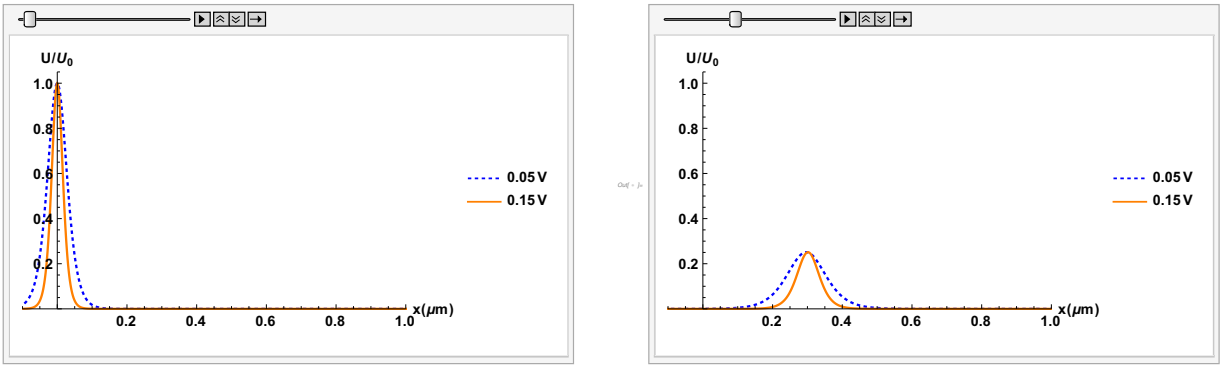

(a) (b)

Figure 16: Snapshots of soliton propagation animation in in-vitro condition at the beginning (a) and at an intermediate (b) distance along the filament. Both input pulses move at same speed.

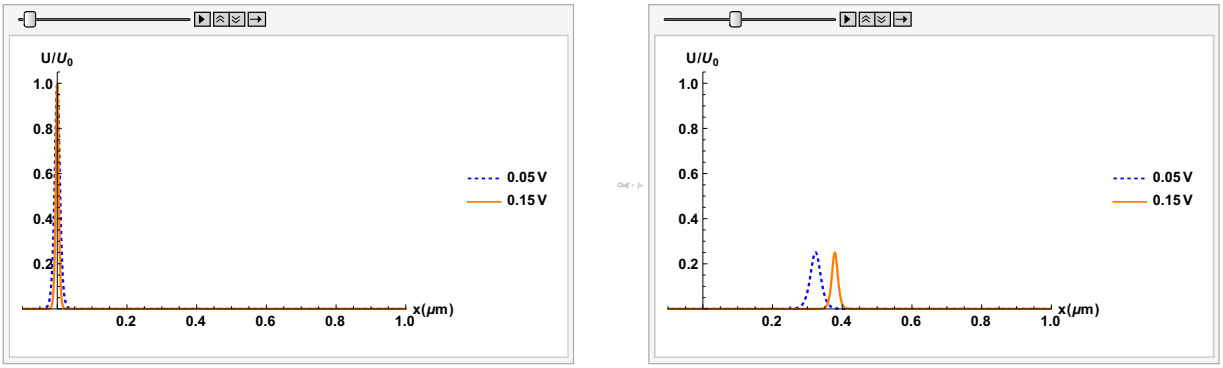

(a) (b)

Figure 17: Snapshots of soliton propagation animation in intracellular condition at the beginning (a) and at an intermediate (b) distance along the filament.

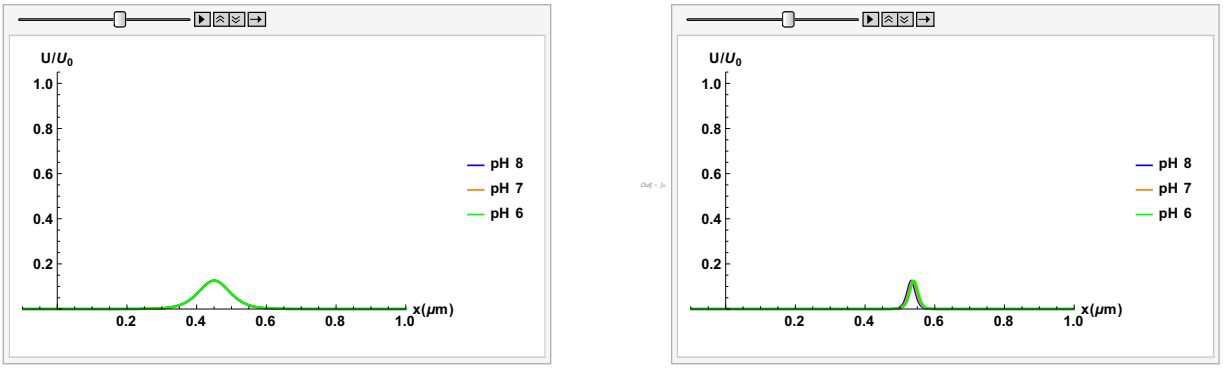

(a) (b)

Figure 18: Snapshots of soliton propagation animation in in-vitro (a) and intracellular conditions at an intermediate (b) distance along the filament.

pathological conditions. In particular, the user has the option of selecting a nucleotide state, isoform of interest and its associated disease. As a unique feature, the investigator may perform a detailed study on the conductivity, mean electric potential, velocity, and peak decay by using an interactive slider for adjustments of the pH (6.0–8.0), and voltage input ($0.05V$–$0.40V$). This simple and easy to use program requires no specialized training or expertise in the field, and is designed to conduct a detailed analysis on both wild-type and mutated conformations. The simplicity of the theoretical formulation, and the high performance of the Mathematica software, enable the analysis of multiple conditions without computational restrictions. These studies may provide an unprecedented molecular understanding on how actin filaments are related to aging and disease, due to a more complete understanding of their electrical properties in both muscle and non-muscle cells [32]. A future version of this program will account for the propagation of divalent ionic waves along actin filaments.

APPENDIX

Theory

In the following sections, we give a general explanation of the multi-scale approach used to produce the results for the interactive computational program. A detailed explanation on the theory can be found in a proceeding article [9].

The atomistic scale (Å)

The residues on the protein and pH of the solution play a large role in the formation of the EDL, which is particularly important for consideration of mutated proteins. To allow for a model that reflects changes at the atomistic scale, we performed titration curves on the most recent actin models in the protein data bank, and used a zeta potential comparison to determine the most accurate description based on the polyelectrolyte nature of actin. The Cong model (3B5U) [21] was then uploaded into the pdb2pqr webserver to determine the pH dependent amino acids exposed on the protein. The volume of the filament was determined by using the "3v: voss volume voxelator" webserver, which was then used to calculate the radius ($R = 23.83$Å), linear charge density (λ), and the surface charge density (σ).

Mutations, isoforms, and nucleotide states

Mutations can be found in all of the six human actin genes, and most often result in a substitution of an amino acid due to the change in a single base pair (missense mutation) [33]. The removal of a pH dependent residue has an effect even at the monomer scale, which is compounded in filament form by the number of added monomers. The replacement of a residue with another pH dependent amino acid will change the capacitance and both resistances for a given pH value.

The monomeric scale (nm)

The intrinsic properties of the actin monomer relate to the charge build up near the surface, and the ionic current next to the polymer. This can be described by an RLC circuit model, where R represents the resistor, C is the capacitor, and L is the inductor. The inductance has been shown to be negligible, and therefore, is not considered in the multi-scale approach [9].

Resistance

Using the surface charge density (σ), Debye length ($\lambda_D = \epsilon RT/(F^2 \sum_i z_i^2 c_i^\infty)$), and dielectric permittivity ($\epsilon = \epsilon_o \epsilon_r$), along with the Bessel function of the second kind, and a linearized approximation of the Poisson-Boltzmann equation allows for the mean electrostatic potential to be expressed as

$$\phi(r) = \frac{\sigma \lambda_D}{\epsilon} \frac{K_0(r/\lambda_D)}{K_1(r_\xi/\lambda_D)} \tag{1}$$

The parameter r_ξ is the position of the zeta potential, and r is a distance from the surface larger than the actin radius. Also, R, T, and F are the gas constant, temperature, and Faraday's constant, respectively. The ionic valence of species i is represented by z_i and the bulk ion concentration is denoted by c_i^∞.

The ionic current is derived from the ionic flow equation $i_z = k(r)E_z + v_z(r)\rho_e(r)$, where k is the conductivity, E_z is the electric field in the longitudinal (axial) direction, v_z is the axial velocity profile and ρ_e is the ionic charge density distribution.

Integration over the ionic flow equation gives the longitudinal current when using r_ξ and $l_B + r_\xi$ as the limits of integration with r as the integration variable ($\int_{r_\xi}^{l_B+r_\xi} dr$), where $l_B = e^2/(4\pi\epsilon_o k_B T)$ is the Bjerrum length. Therefore, we have

$$I_l = E_z \pi((l_B + r_\xi)^2 - r_\xi^2)(k^\infty + \Delta k_l). \tag{2}$$

The conductivity of the bulk solution is represented by $k^\infty = F^2 \sum_i z_i^2 u_i c_i^\infty$, and Δk_l is a novel parameter that represents the longitudinal conductivity in the diffuse layer, and depends on the intrinsic nature of the actin protein, Bjerrum length, as well as the EDL thickness

$$\Delta k_l = -\frac{2F^3 \sigma \lambda_D^2 r_\xi \sum_i z_i^3 u_i c_i^\infty}{\epsilon RT \left[(l_B + r_\xi)^2 - r_\xi^2\right]} \left[1 - \frac{(l_B + r_\xi) K_1\left(\frac{l_B + r_\xi}{\lambda_D}\right)}{r_\xi K_1\left(\frac{r_\xi}{\lambda_D}\right)}\right] + \frac{r_\xi^2 \sigma^2}{\mu\left[(l_B + r_\xi)^2 - r_\xi^2\right]} G(l_B, r_\xi, \lambda_D)$$

with

$$G(l_B, r_\xi, \lambda_D) = \frac{1}{K_1\left(\frac{r_\xi}{\lambda_D}\right)^2} [\left(K_0\left(\frac{r_\xi}{\lambda_D}\right)^2 - K_1\left(\frac{r_\xi}{\lambda_D}\right)^2\right) + \frac{1}{r_\xi}\left(2\lambda_D K_0\left(\frac{r_\xi}{\lambda_D}\right) K_1\left(\frac{r_\xi}{\lambda_D}\right)\right)$$
$$-\left(\frac{(l_B + r_\xi)^2}{r_\xi^2}\left[K_0\left(\frac{l_B + r_\xi}{\lambda_D}\right)^2 - K_1\left(\frac{l_B + r_\xi}{\lambda_D}\right)^2\right]\right) - \left(\frac{2\lambda_D (l_B + r_\xi)}{r_\xi^2} K_0\left(\frac{l_B + r_\xi}{\lambda_D}\right) K_1\left(\frac{l_B + r_\xi}{\lambda_D}\right)\right)]$$

A similar method determines the ionic current in the radial direction as

$$I_r = \frac{2\pi\ell}{ln((l_B + r_\xi)/r_\xi)} \Big(k^\infty + \frac{F^3}{2RT} \sum_i z_i^3 u_i c_i^\infty (\phi(l_B + r_\xi) + \phi(r_\xi))\Big) \Delta\phi. \tag{3}$$

The parameter ℓ is the diameter of an actin monomer, u_i is the ion mobility of species i, $\Delta\phi$ is the EDL voltage drop, and $\Delta k_t = \frac{F^3}{2RT} \sum_i z_i^3 u_i c_i^\infty (\phi(l_B + r_\xi) + \phi(r_\xi))$ is a similar parameter as Δk_l except for in the radial direction.

Using Ohm's law the longitudinal and transversal resistances are

$$R_l = \frac{\ell}{\pi((l_B + r_\xi)^2 - r_\xi^2)\left|k^\infty + \Delta k_l\right|} \tag{4}$$

and

$$R_t = \frac{ln((l_B + r_\xi)/r_\xi)}{2\pi\ell\left|k^\infty + \Delta k_t\right|}, \tag{5}$$

respectively.

Capacitance

Capacitance arises from the build up of counterion charge near its negatively charged surface. Therefore, the short range forces of water crowding, ion size asymmetry, and ion-ion repulsion cannot be ignored. To include these, CSDFT calculations were used for an accurate consideration of the surface electric potential $\psi_o = \phi(R)$. This process was explained in the supplement of a previous work [9], and can easily be done by using JACFC web application [24, 25, 26]. .

The differential capacitance representing a monomer is found to be

$$C_d = \frac{d\sigma}{d\psi_o} = \widehat{C_o}(1 - 2\widehat{b}\psi_o + 3\widehat{c}\psi_o^2 + \mathcal{O}(\psi_o^3)) \tag{6}$$

For the total charge we integrate over the voltage drop and get

$$Q = 2\pi r_\xi \ell \widehat{C_o}(V - bV^2) = VC_o(1 - bV^2) = VC(V) \tag{7}$$

where b characterizes the non-linear behavior of the capacitance.

The filament scale (μm)

The flow of ions $I_l(x,t) = V(x,t)/Z$ along a polymerized actin filament comes from the transfer of ions from one unit cell (actin monomer) to the next. This is accomplished by using Kirchhoff's laws on the discrete transmission line composed of N unit cells, where N represents the number of monomers in the filament. We then use a continuum approximation and a Taylor series expansion to get the perturbed Korteweg-de Vries (pKdV) differential equation

$$\frac{\partial W}{\partial \tau} - 6W\frac{\partial W}{\partial \xi} + \frac{\partial^3 W}{\partial \xi^3} = \mu_2 \frac{\partial^2 W}{\partial \xi^2} - \mu_3 W \tag{8}$$

where $W(\xi,\tau) = \frac{24}{\gamma} Z^{-1/2} V(\xi,\tau) = \frac{24}{\gamma} Z^{1/2} I_l(\xi,\tau)$, $\xi = \frac{x}{\beta} - \frac{t}{\alpha_o}$, $\tau = \frac{t}{24\alpha}, \alpha = C_o Z > 0, \beta = 2\ell$, $\mu_2 = \frac{6R_t}{Z}$ and $\mu_3 = \frac{24R_l}{Z}$.

The approximate analytic solution for the soliton is

$$W(x,t) = -2\left[\Omega(\frac{t}{24\alpha})\right]^2 \text{sech}^2\left(\Omega(\frac{t}{24\alpha})\left[\left(\frac{x}{\beta} - \frac{t}{\alpha}\right) - \eta(\frac{t}{24\alpha})\right]\right) \tag{9}$$

where

$$\eta(\tau) = -\frac{5}{4\mu_2}[4\mu_3\tau + 3\ln(5\mu_3) - 3\ln\left(-4\Omega_0^2\mu_2 + \exp\left(\frac{4\tau\mu_3}{3}\right)\left[4\Omega_0^2\mu_2 + 5\mu_3\right]\right)] \tag{10}$$

and

$$\Omega(\tau) = \Omega_0 \sqrt{\frac{\exp\left(-\frac{4\tau\mu_3}{3}\right)}{1 + \frac{4\mu_2\Omega_0^2}{5\mu_3}\left(1 - \exp\left(-\frac{4\tau\mu_3}{3}\right)\right)}} \tag{11}$$

$\Omega_0^2 = 24V_o/(Z^{1/2}|\gamma|)$ with $\gamma = 3\frac{C_o Z}{bZ^{3/2}C_o}$

The soliton propagation velocity is given by

$$v(\tau) = -\frac{5}{4\mu_2}\left[4\mu_3 - \frac{4\exp\left(\frac{4\tau\mu_3}{3}\right) \times \mu_3\left[4\Omega_0^2\mu_2 + 5\mu_3\right]}{-4\Omega_0^2\mu_2 + \exp\left(\frac{4\tau\mu_3}{3}\right) \times \left[4\Omega_0^2\mu_2 + 5\mu_3\right]}\right]$$

The expression for the impedance is $Z \approxeq \sqrt{R_{equiv}^2 + X_{equiv}^2}$, where $R_{equiv} = R_l + R_t$, $X_{equiv} = T_o^{G-actin}/(2\pi C_o)$, and $T_o^{G-actin}$ characterizes the time scale of the circuit unit.

Other important considerations are the maximum travel distance, average velocity and vanishing time represented by x_{max}, v_{avg}, and t_{max}, respectively. The maximum travel distance is given by

$$x_{max} = |(1 - t_{max}/\alpha)\beta|$$

and the average velocity is

$$v_{avg} = \frac{1}{t_{max}}\int_0^{t_{max}} v(t)dt$$

The vanishing time is the solution of the implicit equation $\Omega^2(t_{max}/(24\alpha)) = 0.01 * \Omega_0^2$, which represents the time when the soliton amplitude attenuates to 1% of its initial amplitude.

Acknowledgements

This work was supported by the National Institutes of Health [grant number 1SC1GM127187].

6. References

[1] Maria Giuseppa Leggio, Laura Mandolesi, Francesca Federico, Francesca Spirito, Benedetta Ricci, Francesca Gelfo, and Laura Petrosini. Environmental enrichment promotes improved spatial abilities and enhanced dendritic growth in the rat. *Behavioural Brain Research*, 163(1):78–90, 2005.

[2] Peter W. Hickmott and Iryna M. Ethell. Dendritic plasticity in the adult neocortex. *The Neuroscientist*, 12(1):16–28, 2006.

[3] Sara Geraldo and Phillip R. Gordon-Weeks. Cytoskeletal dynamics in growth-cone steering. *Journal of Cell Science*, 122(20):3595–3604, 10 2009.

[4] Thomas D. Pollard and John A. Cooper. Actin, a central player in cell shape and movement. *Science*, 326(5957):1208–1212, 2009.

[5] Roberto Dominguez and Kenneth C. Holmes. Actin structure and function. *Annual Review of Biophysics*, 40(1):169–186, 2011.

[6] H.F. Cantiello E.C. Lin. A novel method to study the electrodynamic behavior of actin filaments. evidence for cable-like properties of actin. *Biophysical Journal*, 65(4):1284–1289, 1993.

[7] B. R. Frieden and R. A. Gatenby. Signal transmission through elements of the cytoskeleton form an optimized information network in eukaryotic cells. *Scientific Reports*, 9(1):6110, April 2019.

[8] Pengyu Ren, Jaehun Chun, Dennis G. Thomas, Michael J. Schnieders, Marcelo Marucho, Jiajing Zhang, and Nathan A. Baker. Biomolecular electrostatics and solvation: a computational perspective. *Quarterly Reviews of Biophysics*, 45(4):427–491, November 2012. Publisher: Cambridge University Press.

[9] Christian Hunley, Diego Uribe, and Marcelo Marucho. A multi-scale approach to describe electrical impulses propagating along actin filaments in both intracellular and in vitro conditions. *RSC Adv.*, 8:12017–12028, 2018.

[10] P. G. Drazin and R. S. Johnson. *Solitons: An Introduction*. Cambridge Texts in Applied Mathematics. Cambridge University Press, 2 edition, 1989.

[11] Wolfram Research, Inc. Mathematica, Version 12.3.1. Champaign, IL, 2021.

[12] Kohki Okabe, Noriko Inada, Chie Gota, Yoshie Harada, Takashi Funatsu, and Seiichi Uchiyama. Intracellular temperature mapping with a fluorescent polymeric thermometer and fluorescence lifetime imaging microscopy. *Nature Communications*, 3(1):705, 2012.

[13] Ryuichi Tanimoto, Takumi Hiraiwa, Yuichiro Nakai, Yutaka Shindo, Kotaro Oka, Noriko Hiroi, and Akira Funahashi. Detection of temperature difference in neuronal cells. *Scientific Reports*, 6(1):22071, 2016.

[14] Dominique Chretien, Paule Benit, Hyung-Ho Ha, Susanne Keipert, Riyad El-Khoury, Young-Tae Chang, Martin Jastroch, Howard Jacobs, Pierre Rustin, and Malgorzata Rak. Mitochondria are physiologically maintained at close to 50 c. *PLOS Biology*, 16(1):0, 2018.

[15] D. S. Viswanath, editor. *Viscosity of liquids: theory, estimation, experiment, and data*. Springer, Dordrecht, 2007. OCLC: ocm77482252.

[16] Ove Sten-Knudsen. *Biological membranes: Theory of trans- port, potentials and electrical impulses*. Cambridge Univ. Press., Cambridge, United Kingdom, 2002.

[17] Allan N. Soriano, Arjay M. Agapito, Loui John Lee I. Lagumbay, Alvin R. Caparanga, and Meng-Hui Li. Diffusion coefficients of aqueous ionic liquid solutions at infinite dilution determined from electrolytic conductivity measurements. *Journal of the Taiwan Institute of Chemical Engineers*, 42(2):258–264, 2011.

[18] Wolfram research, interpolation, wolfram language function. https://reference.wolfram.com/language/ref/Interpolation.html, 1991. updated 2008.

[19] P. VANYSEK. Ionic conductivity and diffusion at infinite dilution. *CRC Hand of Chemistry and Physics*, pages 5–92, 1993.

[20] D G Miller. Estimation of tracer diffusion coefficients of ions in aqueous solution. 9 1982.

[21] Yao Cong, Maya Topf, Andrej Sali, Paul Matsudaira, Matthew Dougherty, Wah Chiu, and Michael F. Schmid. Crystallographic conformers of actin in a biologically active bundle of filaments. *Journal of Molecular Biology*, 375(2):331 – 336, 2008.

[22] Laurent Schwartz, Sabine Peres, Mario Jolicoeur, and Jorgelindo da Veiga Moreira. Cancer and alzheimers disease intracellular ph scales the metabolic disorders. *Biogerontology*, 21(6):683–694, 2020.

[23] Salvador Harguindey, Daniel Stanciu, JesÃºs Devesa, Khalid Alfarouk, Rosa Angela Cardone, Julian David Polo Orozco, Pablo Devesa, Cyril Rauch, Gorka Orive, Eduardo Anitua, SÃ©bastien Roger, and Stephan J. Reshkin. Cellular acidification as a new approach to cancer treatment and to the understanding and therapeutics of neurodegenerative diseases. *Seminars in Cancer Biology*, 43:157–179, 2017. The new pH-centric Anticancer Paradigm in Oncology and Medicine.

[24] M. marucho, university of texas at san antonio. http://neuronanobiophysics.utsa.edu. online; accessed 19-Jul-2021.

[25] Marcelo Marucho. A java application to characterize biomolecules and nanomaterials in electrolyte aqueous solutions. *Computer Physics Communications*, 242:104–119, 2019.

[26] Marcelo Marucho. Java application for cytoskeleton filament characterization (JACFC). *Software Impacts*, 8:100072, May 2021.

[27] Francine Parker, Thomas Baboolal, and Michelle Peckham. Actin mutations and their role in disease. *International Journal of Molecular Sciences*, 21(9):3371, 2020.

[28] Dmitri S. Kudryashov and Emil Reisler. Atp and adp actin states. *Biopolymers*, 99(4):245–256, 2013.

[29] Benjamin J. Perrin and James M. Ervasti. The actin gene family: Function follows isoform. *Cytoskeleton*, 67(10):630–634, 2010.

[30] Kristen Nowark, Gianina Ravenscroft, and Nigel Laing. muscle alpha-actin diseases (actinopathies) pathology and mechanisms. *Acta Neuropathological*, 125(1):19–32, 2013.

[31] H.F. Cantiello, C. Patenaude, and K. Zaner. Osmotically induced electrical signals from actin filaments. *Biophysical Journal*, 59(6):1284 – 1289, 1991.

[32] Nancy Woolf, Avner Priel, and Jack Tuszynski. *Nanoneuroscience: Structural and Functional Roles of the Neuronal Cytoskeleton in Health and Disease*. Springer, Verlag New York, 2009.

[33] Henderson CA, Gomez CG, Novak SM, Mi-Mi L, and Gregorio CC. Overview of the muscle cytoskeleton. *Comprehensive Physiology*, 7(3):891–944, 2017.